MAGNETIC RESONANCE IN CHEMISTRY
*Magn. Reson. Chem.* 2005; **43**: S248–S255
Published online in Wiley InterScience (www.interscience.wiley.com). DOI: 10.1002/mrc.1681

MRC

# Pulsed 180-GHz EPR/ENDOR/PELDOR spectroscopy†

**M. M. Hertel, V. P. Denysenkov, M. Bennati and T. F. Prisner***

Institute for Physical and Theoretical Chemistry and Center for Biomolecular Magnetic Resonance, J. W. Goethe-University, Frankfurt am Main, Germany

Received 2 May 2005; Revised 15 June 2005; Accepted 17 June 2005

**Within this review, we describe a home-built pulsed electron paramagnetic resonance (EPR) spectrometer operating at 180 GHz as well as the incorporation of two double resonance techniques, electron nuclear double resonance (ENDOR) and pulsed electron double resonance (PELDOR), along with first applications. Hahn-echo decays on a TEMPO/polystyrene sample are presented, demonstrating that the observation of anisotropic librational motions is possible in a very precise manner at high magnetic fields. Bisdiphenylene-phenyl-allyl is used as a model system to illustrate the performance of the setup for $^1$H-ENDOR using the Mims as well as the Davies sequence. Furthermore, first $^1$H-Mims and Davies ENDOR spectra on a biological sample, the wild-type Ras•$Mn^{2+}$•GDP protein, are reported. The capability of the 180-GHz PELDOR setup is demonstrated using the three-pulse ELDOR sequence on the protein ribonucleotide reductase (RNR) subunit R2 from *Escherichia coli*, which contains two tyrosyl radicals at a 33 Å distance. At 180 GHz, orientation selectivity is observed and the modulation frequency is found to be in good agreement with theoretical predictions. Copyright © 2005 John Wiley & Sons, Ltd.**

**KEYWORDS:** High-field/high-frequency pulsed EPR; ENDOR; PELDOR; DEER; librational motion; Ras•$Mn^{2+}$•GDP; tyrosyl radical

## INTRODUCTION

In the past two decades, the implementation of high-field electron paramagnetic resonance (HF-EPR) spectrometers has been greatly facilitated by substantial progress in microwave technology. The first pulsed HF-EPR spectrometer was built in 1989 in Leiden at 95 GHz,[1] followed by two spectrometers operating at 140 GHz built in Moskau[2] and in Cambridge[3] along with another 95-GHz spectrometer built later on in Berlin.[4] Since 1996, a 95-GHz pulsed HF-EPR spectrometer has been available commercially at Bruker Analytik,[5] as well as at the Donetsk Physico Technical Institute, along with a 95- and 130-GHz pulsed EPR spectrometer.[6,7] The vast application potential of high-frequency EPR and the advantages of pulsed vs continuous wave (cw) techniques have been documented in several recent review articles and books.[8,9] Only two home-built spectrometers that permit routine spectroscopy have been reported so far at microwave frequencies higher than 140 GHz, the first one at 180 GHz[10] and the second at 270 GHz.[11] The possible extension to even higher frequencies has been demonstrated at 604 GHz using pulsed far infrared lasers.[12]

It is well established that electron nuclear double resonance (ENDOR) spectroscopy shows considerable advantages when performed at high fields and frequencies.[6,13–15,37] The first pulsed high-field W-band ENDOR spectrometer operating at 95 GHz was built simultaneously in Berlin[4] and in Leiden[14] in 1995. In 1999, another pulsed W-band ENDOR spectrometer was implemented in Rehovot[6] and, at the same time, at a frequency of 140 GHz in Cambridge.[13] Very recently, pulsed ENDOR at 275 GHz has been demonstrated in Leiden.[16] One of the numerous advantages of performing ENDOR at high fields is the increased nuclear Zeeman resolution, which leads to the separation of ENDOR signals from different nuclei as well as significant simplification of the ENDOR spectra to first order. Another advantage is the possibility to determine the sign of hyperfine coupling constants (HFCs) by exploiting the large thermal electron spin polarization at high fields and low temperatures.[17,18] Furthermore, the increased resolution of $g$-anisotropy at high fields allows the selective excitation of specific molecular orientations. For high-spin systems, such as $Mn^{2+}$,[19] HF-EPR offers the crucial advantage of reducing the forbidden transitions and narrowing the central transitions ($m_S = -1/2 \rightleftarrows +1/2$).

The incorporation of a pulsed electron double resonance (PELDOR) unit into a pulsed EPR spectrometer and the performance of the PELDOR experiment itself is more difficult at high magnetic fields than at standard X-band frequencies for various reasons. First, the implementation of a second frequency channel in the high-frequency microwave bridge without degrading the pulse performance of the spectrometer is much more demanding. Further, the limited available microwave power renders the pumping pulse more selective. The first ELDOR experiment reported at high fields was performed at the Massachusetts Institute of

†**Presented as part of a special issue on High-field EPR in Biology, Chemistry and Physics.**

*Correspondence to: T. F. Prisner, Institute for Physical and Theoretical Chemistry, Marie-Curie-Str. 11-13, 60439 J.W.G.-University, Frankfurt am Main, Germany.
E-mail: prisner@chemie.uni-frankfurt.de

Technology (MIT) using a gyrotron as a microwave pumping source.[20] This setup was used to measure cross-relaxation in a homogeneously broadened EPR line. However, such high-power microwave sources are not standard components of HF-EPR spectrometers. For distance measurements, the low efficiency of the pump pulse combined with the fact that EPR lines at higher fields usually become much broader because of *g*-anisotropy leads to the expectation that the modulation effect will be much weaker than that observed at X-band. On the other hand, the experimental conditions at high fields allow the performance of orientation-selective experiments, which can additionally provide the relative molecular orientation of the two radicals with respect to each other. Recently, we have reported the first PELDOR experiment at high fields on a biological sample.[21]

Within the present review, we describe the main features and latest developments of our 180-GHz pulsed EPR/ENDOR/PELDOR spectrometer. The performance of the pulsed EPR setup is demonstrated with a two dimensional $T_2$ relaxation measurement on a TEMPO (2,2,6,6-tetramethylpiperidin-1-oxyl) radical showing the anisotropic librational motion of the molecule. The feasibility of the double resonance experiments is illustrated, presenting first applications on biological systems.

## TECHNICAL DESCRIPTION OF THE DOUBLE RESONANCE EPR SPECTROMETER

### Pulsed EPR spectrometer

The spectrometer consists of the superconducting magnet, the HF-microwave bridge and a data acquisition system. The microwave bridge contains the sources and detectors, a quasioptical circulator and the probehead for pulsed EPR/ELDOR or ENDOR experiments (Fig. 1).

A cryomagnet from Oxford Instruments is used to produce the external magnetic field. The superconducting magnet consists of two coils. The main coil produces a center magnetic field in the range of 0–7 T. The sweep coil can be used to sweep the magnetic field in the range of 0.15 T with a maximum speed of 3 mT $s^{-1}$. The accuracy of setting the magnetic field value is 0.2 mT without using an internal *g*-standard. Liquid helium from the helium bath is used for temperature control between 3.3 and 278 K. The temperature at the sample is regulated by a liquid helium flow, which is pumped out of the helium bath through a capillary into the sample space where the liquid helium is warmed by a heater. Temperature control is performed by an ITC503 temperature controller with a stability of 0.01 K at 3.3 K.

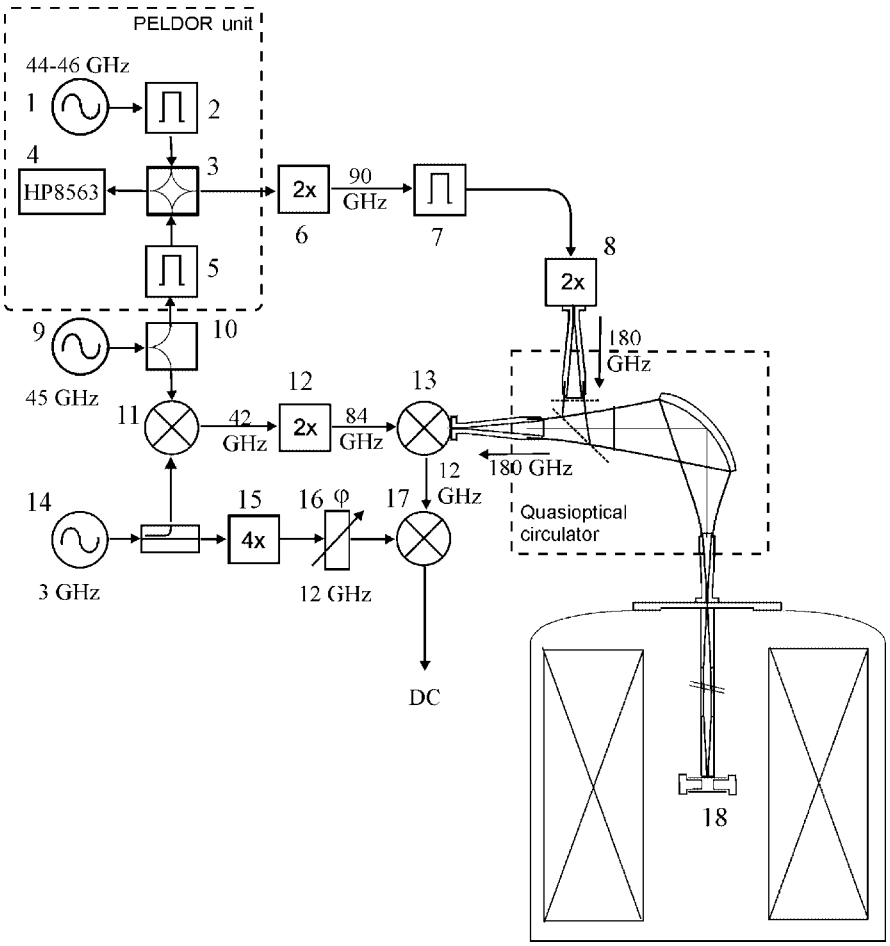


**Figure 1.** Block diagram of the 180-GHz pulsed EPR/ELDOR spectrometer. (1) Variable frequency oscillator; (2), (5), (7) fast switches; (3) magic-T; (4) spectrum analyzer; (6), (8), (12) frequency doublers; (9), (14) master oscillators; (10) power divider; (11), (13), (17) mixers; (15) frequency multiplier; (16) phase shifter; (18) resonant cavity. 45-GHz amplifiers (injection locked oscillators) are not shown in the figure for simplification.

### *EPR and ELDOR microwave bridge*

The microwave bridge is built according to a heterodyne phase-sensitive detection scheme.[10] A 45-GHz Gunn oscillator is used as a master oscillator for driving the transmitter as well as for the local oscillator for the subharmonic mixer. The bridge is extended for performing two-frequency experiments by inserting an additional oscillator into the transmitter at the 45-GHz stage, before the frequency multiplication chain. The second microwave frequency is generated by a Gunn oscillator (Cernex) and can be tuned manually in the range 44–46 GHz to adjust the desired spectral pumping position. The pulses at both frequencies are formed independently in two separate channels and are combined via a magic-T into the multiplication/amplification stages of the transmitter. All switches are driven and synchronized by a pulse generator (Tektronix P3420), which is controlled by a PC. The exact frequencies of the pump and probe pulses are monitored with an HP8563 spectrum analyzer connected to the fourth port of the magic-T. The microwave power at 180 GHz, which amounts to 20 mW at the transmitter output, is fed into the quasioptical circulator and finally reaches the probehead.

### *EPR and ELDOR probehead*

The probehead, as illustrated in Fig. 2, is equipped with an elliptical mirror (1), which reflects the incoming signal through a sealed Teflon window (7) into a low losses corrugated waveguide (2). The waveguide has a tapered end to the cylindrical cavity operating in $TE_{011}$ mode. The cavity consists of a cylinder tube (3) of 2.2 mm i.d. with an iris of 0.4 mm diameter and two plungers (4, 5). The assembly allows critical coupling when measuring frozen solutions of biological samples. Plunger (5) can be moved along the cavity tube, whereas plunger (4) is in a fixed position. This fixed position is chosen such that both plungers have the same distance to the iris when the resonator containing a frozen sample is tuned to 180 GHz. The resonant frequency of the cavity can be tuned by turning a rod (6) around its axis from outside the cryomagnet. Samples can be introduced into the cavity through the 0.4-mm slot along the axis of the fixed plunger. Owing to small losses through the quasioptics and the corrugated waveguide (less than 1.5 dB), the microwave power incident to the cavity was measured to be about 15 mW.

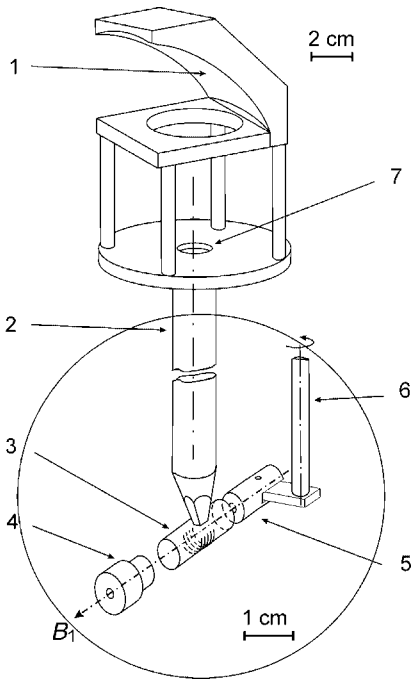


**Figure 2.** EPR probehead design. (1) Elliptical mirror, (2) corrugated waveguide, (3) resonant cavity, (4) fixed plunger, (5) moveable plunger, (6) driving rod, (7) sealed Teflon window.

The pulsed sensitivity of the system was tested using TEMPO (2,2,6,6-tetramethylpiperidin-1-oxyl), which was dissolved in a mixture of water/glycerol (6/4) in order to achieve a glassy frozen state. The sensitivity measurements were all carried out at 15 K. The sensitivity of a pulsed spectrometer can be calculated via[9]:

$$E = \frac{n}{S/N \cdot \Delta B_{1/2}} \, e^{-\frac{2\tau}{T_2}},$$

where $S/N$ is the signal-to-noise ratio at maximum signal intensity in single shot, $\Delta B_{1/2}$ is the inhomogeneous line width, $\tau$ is the pulse spacing time, $T_2$ is the transverse relaxation time and $n$ is the number of spins in the sample. We obtain a sensitivity of $\sim 1 \times 10^{10}$ spins/G in pulsed mode at 15 K. With 15 mW incident power at the cavity, we achieve a $\pi/2$-pulse length of 50–70 ns for a 1/2 spin, corresponding to a $B_1$ of approximately 0.16 mT. The quality of the loaded resonator is about $Q_{\text{loaded}} \sim 1000$–$2000$. The conversion factor was calculated according to

$$c = \frac{B_1}{\sqrt{P_{\text{MW}} \cdot Q}}$$

to be about 0.03 mT/$\sqrt{W}$.

In order to detect short-lived radical intermediates in enzymatic reactions, it is necessary to keep the samples frozen during the insertion process into the cryostat. This represents a major challenge with high-frequency spectrometers because of the miniature size of the cavity and the sample tubes. For this special purpose, we developed plungers made out of G10, a fiberglass-based laminate, for which the ends facing the cavity were plated with a copper cap. With this setup, we were able to freeze quench and detect a radical intermediate in the reduction of benzoyl CoA via benzoyl CoA reductase.[22]

## 180-GHz ENDOR

### *RF system and circuit*

The radio frequency (RF) transmitter unit, consisting of an RF synthesizer (Rohde and Schwartz), a high-speed PIN switch with 5 ns rise/fall time (Synergy Microwave Corporation) and an RF amplifier (Dressler) with 400 W pulsed power, was incorporated into the pulsed EPR spectrometer described in the section 'Pulsed EPR Spectrometer'. The probehead for ENDOR experiments was equipped with a broadband RF circuit, consisting of an RF coil terminated with a 30-dB high-power attenuator (Weinschol Associates) used as a 50 Ω load. The RF coil is a four-turn flat coil with an inner diameter of

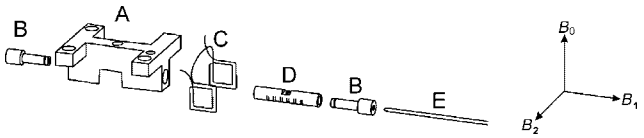


**Figure 3.** Schematic drawing of the 180-GHz ENDOR cavity holder (A) with plungers (B), four-turn flat RF coil made of copper wire (C), silver plated, cylindrical $TE_{011}$ cavity (D) and sample tube (E).

approximately 3 mm, made out of insulated 0.5-mm copper wire. This setup allows typical $^1$H $\pi$-pulses of 25 to 30 μs.

*ENDOR probe*

The cylindrical $TE_{011}$ cavity was modified for ENDOR experiments to allow RF penetration by introducing six slots of 0.3 mm width, 0.75 mm apart (Fig. 3). The choice of the distance between the slots and their width was a compromise between minimizing losses of microwave power and maximizing RF penetration. The losses of microwave power originating from the slots were partly compensated for by coating the cavity with a silver layer. The quality of the slotted resonator was measured to be $Q_{\text{loaded}} \sim 600-1200$. For this cavity, we achieve 90° pulse lengths of 70–90 ns, corresponding to a $B_1$ of 0.11 mT at the sample. In order to reduce Eddy currents and heating effects, the cavity holder as well as the two plungers were made out of G10 with copper caps at the ends facing the cavity.

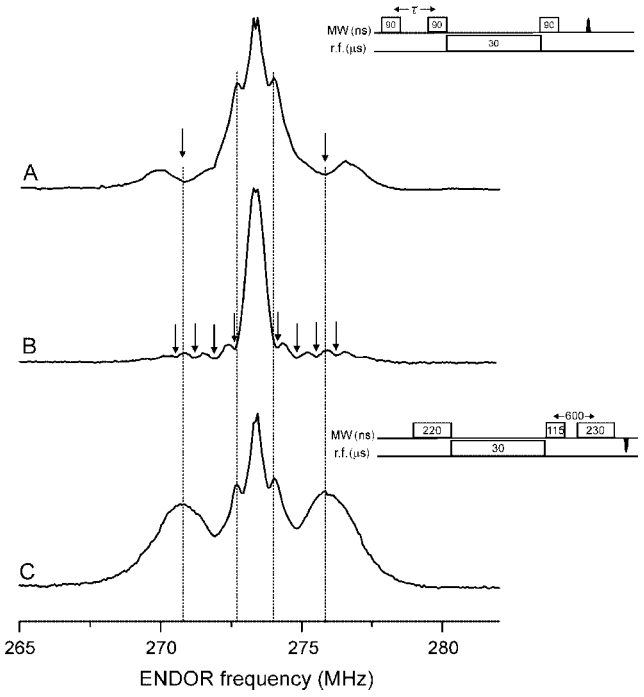


**Figure 4.** $^1$H-Mims (A and B) and Davies (C) ENDOR spectra of BDPA in polysterene measured at 180 K, with 128 shots per point shots using the pulse sequence shown in the inset. The holes created by the polarization pattern by the Mims ENDOR preparation sequence are observed for two different $\tau$-values, 200 and 700 ns (A and B respectively), as indicated by the arrows.

*Performance of the setup for $^1$H-ENDOR*

Mims and Davies ENDOR on BDPA in polystyrene were used to test the performance of $^1$H-ENDOR. The Davies sequence is sensitive to couplings larger than about 5 MHz, and the maximum ENDOR effect is obtained using selective, long pulses.[23] In contrast, Mims ENDOR is used for couplings smaller than 5 MHz. Typical pulse lengths are 70–90 ns for microwave $\pi/2$-pulses in a Mims ENDOR experiment and 25–30 μs for RF $\pi$-pulses. The single-scan $^1$H-ENDOR spectra shown in Fig. 4 were acquired at 180 K with 128 averages/point, using the pulse sequences shown in the inset. In order to demonstrate the effect of the preparation pulses on the polarization pattern for the Mims ENDOR sequence, spectra were recorded for two different $\tau$-values. Blind spots are observed at ±2.5 MHz and $\pm n0.7$ MHz for $\tau = 200$ and 700 ns respectively according to $\varpi = 2n\pi/\tau$. In BDPA, two sets of magnetically equivalent protons lead to one small and one large hyperfine splitting ($A_1 = 1.4$ MHz and $A_2 = 5.0$ MHz),[13] indicated by the dotted lines in Fig. 4. It is known that the Mims ENDOR effect on the matrix line is very sensitive to the $\tau$-value.[24] We find an ENDOR effect of ∼25 vs ∼75% of the echo amplitude when going from $\tau = 200$ to 700 ns. In comparison, an ENDOR effect of ∼25% is observed when using the Davies pulse sequence.

## APPLICATIONS

### Pulsed EPR relaxation measurements on the TEMPO radical

Pulsed high-field EPR is a versatile tool to probe spin or molecular dynamics compared to cw- and pulsed low-field EPR spectroscopy.[25] One reason for this is the fact that static broadening mechanisms often dominating the line-shape of disordered samples are suppressed. Furthermore, the spectral resolution at high fields, which allows the performance of orientational selective measurements, strongly increases the possibility to resolve the anisotropy of the relaxation with respect to the molecular axis system. From this orientation dependence, the tensorial interactions relevant for the relaxation process can be identified much more easily. This is demonstrated in the following example, where we investigate the small-angle librational motion of a TEMPO radical in a disordered glassy matrix at low temperatures via the transverse relaxation enhancement by this motion. The $T_2$ relaxation traces as a function of the pulse separation time $\tau$ (1st dimension) and of the external magnetic field $B_0$ (2nd dimension) are shown in Fig. 5. The $g$-anisotropy and the $z$-component of the nitrogen hyperfine tensor are clearly resolved at 180 GHz, and the anisotropy of the relaxation can easily be spectrally resolved.

Since ESEEM effects are usually not observed at high magnetic fields, the memory time $T_M$ of the echo decay function can be determined straightforward. Figure 6 shows the measured memory time $T_M$ plotted as a function of the spectral position. A strong anisotropy of the transverse relaxation time as a function of the spectral position can be observed. The fact that the relaxation time is related to the $g$- and hyperfine tensor axis of the nitroxide can be seen very well, especially at the high-field edge of the spectra.

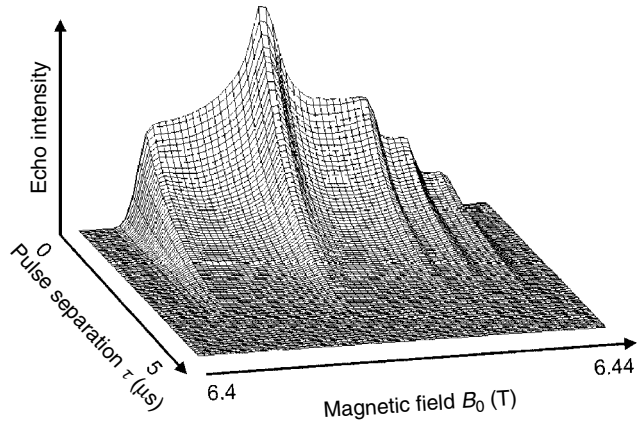


**Figure 5.** Field-swept two-pulse echo decay of a TEMPO nitroxide sample measured at 180 GHz and 30 K. The *g*-matrix-resolved powder spectra as well as the large component of the nitrogen hyperfine coupling $A_{zz}$ at the high-field edge of the spectra can be seen.

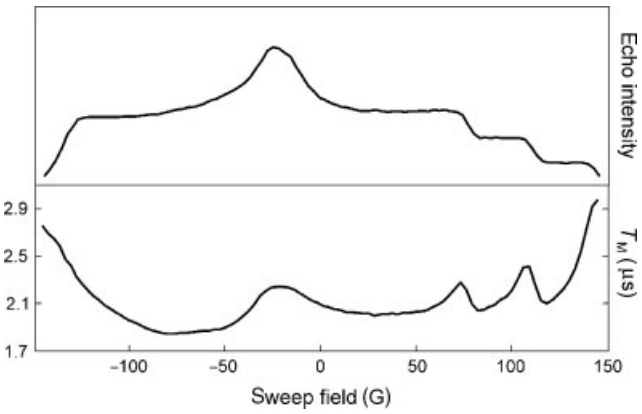


**Figure 6.** Hahn-echo decay memory time $T_M$ as a function of spectral position. Upper trace: field-swept echo-detected spectra measured at 30 K with pulse lengths of 110 ns for the shortest chosen pulse separation time $\tau$ of 140 ns. Lower trace: respective 1/e decay time of the echo signal.

The molecules with the molecular plane perpendicular to the magnetic field (molecular *z*-axis) show up at three distinct spectral positions, split by the large $A_{zz}$ hyperfine coupling. For these spectral positions, a larger $T_M$ value can clearly be observed compared to close by spectral positions with different molecular orientations. In a similar way, the other two **g**-matrix main axis orientations $g_{yy}$ and $g_{xx}$ show maxima in the transversal relaxation time.

## ENDOR on Ras•$Mn^{2+}$•GDP

Ras is a GTP-hydrolizing protein, which is found mutated in about 25–30% of all human tumors.[26] It occurs in two states, a GDP-bound inactive state and a GTP-bound active state. The nucleotide-binding site contains a sixfold coordinated divalent $Mg^{2+}$ ion, which can be substituted by a paramagnetic $Mn^{2+}$ to permit EPR and ENDOR spectroscopy. In the past, we have demonstrated that high-field EPR in liquid solution revealed important differences in the number of water ligands between the wild-type and the G12V oncogenic mutant of the protein in both switch states.[27,28] We have recently employed pulsed ENDOR spectroscopy at 94 GHz to investigate these differences in more detail.[29] Here, we present the first representative application of 180-GHz pulsed $^1$H-ENDOR in the study of Ras•$Mn^{2+}$•GDP. $^1$H couplings are expected from the bound water molecules as well as from the protons of the surrounding amino acids and from the second solvation shell.

Mims and Davies ENDOR spectra of the Ras•$Mn^{2+}$•GDP complex (wild type) were acquired at 4 K and are shown in Fig. 7. The experimental parameters are described in the figure caption. In the Davies ENDOR spectrum, at least two singularities at ±1.25 and ±3.75 MHz, which translate into couplings of ~2.5 and ~7.5 MHz, are observed. Mims ENDOR was used to better resolve the HFCs in the range of ~3 MHz. Here, one observes additional splittings of 2.6, 2.1 and 1.4 MHz.

In the following, the observed patterns are compared with experimental hyperfine couplings of protons located in the surroundings of $Mn^{2+}$ in biological and model systems reported in the literature.

One finds very good agreement of the splittings in the Davies spectrum with HFCs reported in the literature for directly bound water in the $[Mn(H_2O)_6]^{2+}$ complex, for which the reported values vary within the range of $2.0 \leq A_{\perp} \leq 2.5$ MHz and $7.3 \leq A_{||} \leq 8.2$.[17,30,31] The

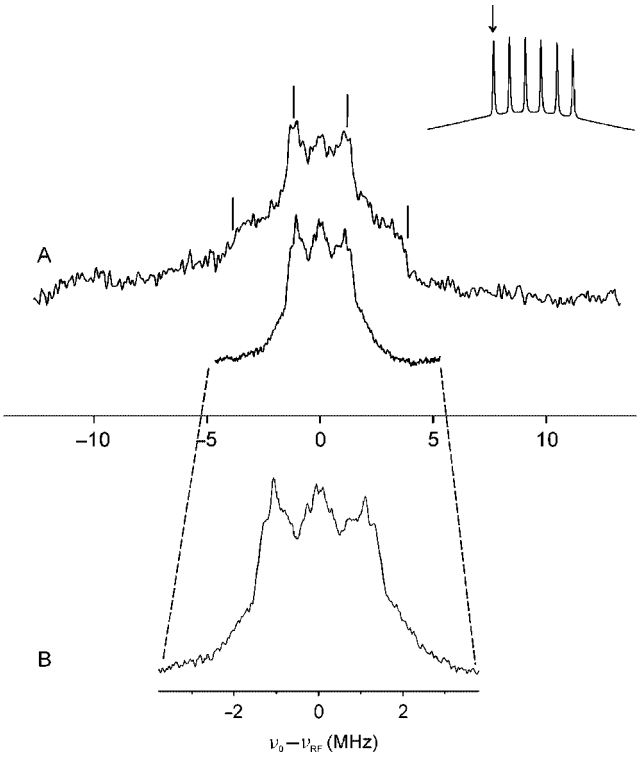


**Figure 7.** $^1$H-Davies (A) and Mims (B) ENDOR spectra of Ras(wt)•$Mn^{2+}$•GDP (~1 mM) measured at the field position indicated by the arrow in the inset showing the field-swept, echo-detected EPR spectrum. Experimental parameters: $T = 4$ K, $t_{RF} = 20$ μs, SRT = 10 ms, RF power = 400 W; Mims: $t_{\pi/2} = 40$ ns, $\tau = 125$ ns, 9 scans with 128 shots per point; Davies: $t_{1\pi} = 150$ ns, $t_{2\pi} = 140$ ns, $\tau = 500$ ns, 4 scans with 32 shots per point.

observed coupling of ~7.5 MHz also agrees well with reported HFCs for directly bound water in *Concanavalin A* (5.4 to 8.2 MHz). Larger couplings $2.9 \leq A_{\perp} \leq 4.3$ MHz observed in *Concanavalin A* from bound water[32] could not be found in the present spectra. We tentatively assign our couplings to directly bound water, with $A_{\perp} \sim 2.5$ MHz and $A_{||} \sim 7.5$ MHz.

The interpretation of the peaks observed in the Mims ENDOR spectrum (2.6, 2.1 and 1.4 MHz) is less evident. Assuming a purely dipolar coupling mechanism, one can estimate the point-dipole distances of these protons. The calculated distances of 3.1 to 3.8 Å lie in the range of protons from surrounding amino acids, as was found in *Concanavalin A* ($A_{\perp} \sim 2.0$ MHz)[32] as well as of water molecules in the second solvation shell. However, they also lie in the range of hyperfine couplings reported in the literature for directly bound water.[30] Smaller peaks observed on the central peak could arise either from further distant amino acids or from water protons in the second solvation shell, as found by studies of the $[Mn(H_2O)_6]^{2+}$ complex (0.5 and 1.0 MHz) by Morrissey *et al*.[30]

## PELDOR on RNR

The PELDOR experiment, described first by Milov *et al*.[33] consists of a two-pulse Hahn-echo with a fixed delay $\tau$ at the observer frequency $\nu_A$ and an additional pump pulse of a flip angle $\pi$ at a different frequency $\nu_B$ and with a variable delay time $T$ with respect to the first pulse of the observer sequence (Fig. 8). Thus, for a spin pair $AB$, the detection occurs on spin $A$, whereas pumping is achieved at the second frequency $\nu_B$ on spin $B$. The PELDOR effect is recorded as a modulation of the amplitude in the spin-echo signal $V$ as a function of the time position $T$ of the pump pulse.

The PELDOR experiment was performed using a solution (approx. 1 mM) of the protein subunit R2 of *Escherichia coli* ribonucleotide reductase (RNR). R2 is a homodimer that contains two tyrosyl radicals ($Y^{\bullet}$) with a distance of 33 Å.[34,35] Experimental results were compared with calculated frequencies predicted from the relative orientations of the radicals obtained from X-ray data.

The time traces were recorded using the three-pulse sequence displayed in Fig. 8, pumping at a fixed resonance position in the EPR powder spectrum corresponding to the maximal signal amplitude ($B||g_2$) and varying the resonance position of detection (Fig. 9). The two-pulse echo spacing $\tau$ between preparation and detection pulses was set to

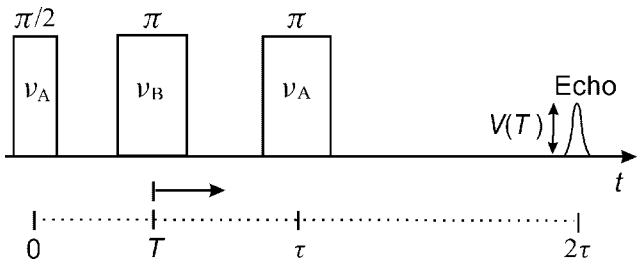


**Figure 8.** Three-pulse ELDOR sequence. $\nu_A$ – detection frequency, $\nu_B$ – pumping frequency, $\tau$ – time distance between preparation and detection pulses, $T$ – current position of pump pulse in time.

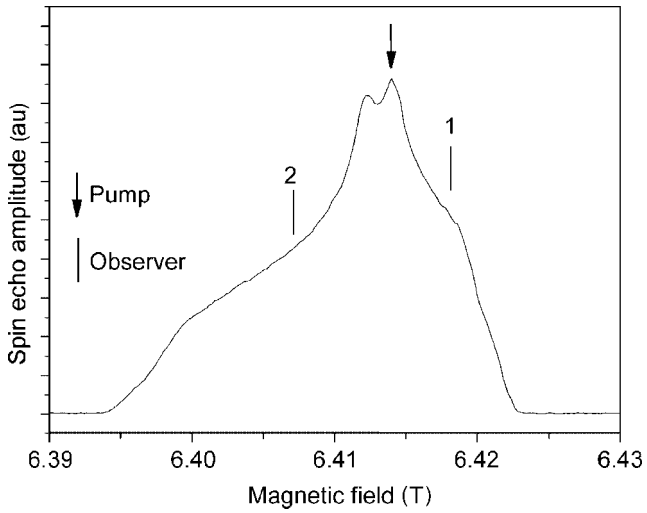


**Figure 9.** 180-GHz echo-detected EPR spectrum of the tyrosyl radicals in RNR-R2 with marked pump and detection positions in the PELDOR experiments.

2.5 μs. The pulse sequence repetition time was 40 ms. Since the detection frequency of the microwave bridge is fixed ($\nu_A = 180$ GHz), the two different resonances of detection were set by adjusting the external magnetic field values. This led to the following experimental settings: Position #1, $B = 64\,185$ G, $\nu_B = 180.1$ GHz; Position #2, $B = 64\,080$ G, $\nu_B = 179.8$ GHz.

The resonant cavity was tuned to the observer frequency $\nu_A$ of 180 GHz. As a result, the pumping frequency is aside from the resonant dip of the cavity, leading to a decreased efficiency of the pump pulse. Despite this drawback, such tuning provided the best sensitivity for spin-echo detection and was the best approach for small echo amplitudes due to significant time spacing $\tau$ with respect to relaxation time. The microwave $\pi$-pulse length at $\nu_A$ of about 100 ns corresponds to a bandwidth of approximately 10 MHz. The length of the pumping pulse at $\nu_B$ was also set to 100 ns. All measurements were performed at 3.3 K.

Time-domain PELDOR traces for detection at two different positions in the EPR line and pumping at $B||g_2$ are presented in Fig. 10(a). The traces show oscillations superimposed on the echo decay. The echo decays were fitted with second-order polynomials and subtracted from the time-domain traces. The frequency-domain spectra were obtained after Fourier transformation (FT) without further manipulation (Fig. 10(b)). The largest PELDOR response (modulation effect) is observed when detecting at $B = 64\,185$ G (Position #1). The FT spectrum shows a modulation frequency peak at 2.3 MHz that is close to the $D_{||}$ value of 2.88 MHz measured at X-band.[34] The reason for not observing the maximum expected $D_{||}$ value is intrinsic. It arises from the fact that in our case the **g**- and **D**-tensors are not collinear and we are not pumping and detecting pairs whose dipolar axis is parallel to the $z$-direction. Changing the detection position below $B||g_2$ (Position #2), the modulation effect almost vanishes and only a weak peak around 1.2 MHz appears. The echo decays display an unusual nonexponential behavior because of slight changes of the last pulse, depending on the position of the pump

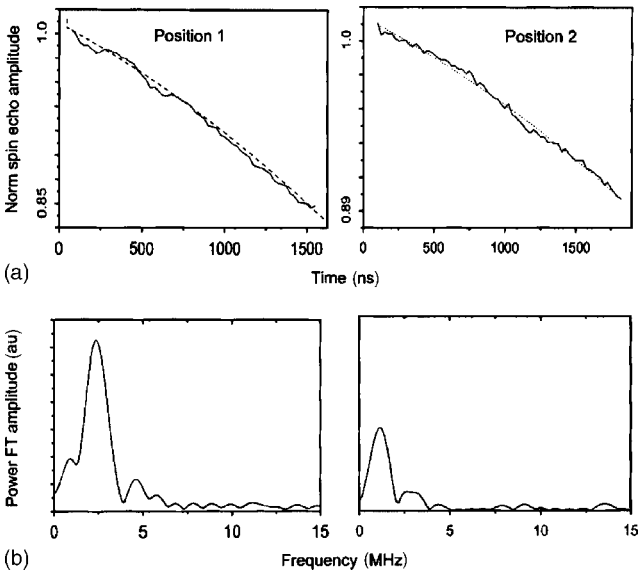


**Figure 10.** (a) PELDOR time traces; (b) Fourier transformation of the frequency-domain PELDOR signal after subtraction of the decay.

pulse. We assume that the output of the last stage of the 45-GHz ILO (injection locked oscillator) situated between the magic-T (3) and the doubler (6) is phase sensitive with respect to the time between pumping and detection pulses.

The results present intrinsic features of a PELDOR experiment dominated by orientational selectivity, which causes that any dipolar frequency between the principal values of the dipolar tensor can be observed. Furthermore, the analysis of the observed frequency is aggravated by the fact that the modulation depth is also a function of the field setting. A detailed calculation, reported in Denysenkov *et al.*,[21] based on the known coordinates of the two tyrosines from the X-ray structure and on the values of the dipolar tensor from X-band PELDOR[34] was employed to rationalize the observed frequencies. In good agreement with the experiment, we found that detection around $B||g_3$ (high-field site) leads to PELDOR frequencies of up to 2.2 MHz and provides the largest contribution of spin pairs. In contrast, detection at $g_1 < g < g_2$ is characterized by a much smaller fraction of spin pairs corresponding to a much weaker PELDOR effect. The calculated PELDOR frequency for detection of Position #2 was 1.1 MHz in agreement with our experiment.

Our comparative experiments at X- and G-band show that distances can be obtained more easily in the X-band experiment rather than in the high-field experiment; however, only at high fields one might be able to extract information about the relative orientation of two radicals. This can lead to a very important structural information in biological systems when studying unknown protein–protein interactions using spin labels or endogenous radicals.

## SUMMARY

As demonstrated by our applications of high-field pulsed EPR, ENDOR and PELDOR, the sensitivity is high enough for performing such experiments on biological samples with broad spectral lines. For pulsed high-field EPR applications, the use of several frequencies in the range of 90–260 GHz will be very important to obtain unambiguous interpretation of relaxation data and details of molecular rotational motion. Additionally, the use of several high frequencies will allow the improved separation of spectral components with different magnetic field dependencies, which are not well resolved spectrally, even at such high magnetic field values. Whereas for ENDOR experiments optimum experimental conditions can already be achieved with the current technology of pulsed high-field spectrometers ($B_1$ and $B_2$ field strengths, relaxation times, spin polarizations and high-field condition), at least for large gyromagnetic ratio nuclei, this condition is only reached in rare cases for pulsed EPR[36] or PELDOR applications. New developments in medium or high-power microwave sources and amplifiers will increase this performance with respect to excitation field strength and pulse lengths. Especially for high-field PELDOR experiments, which could allow the obtaining of additional orientation information on bi- or triradical systems, increased pumping efficiency would strongly improve the possibilities and applicability of the method. The advantage of a much smaller sample volume at high fields, especially important for biological samples that are difficult to harvest or to purify, is contrasted by the increasing difficulties in handling and storing the samples under low-temperature or air-free conditions. We could show that cold loading of the samples is possible with our setup, but more sophisticated sample cells and resonators might be needed at higher microwave frequencies.

## Acknowledgements

The authors gratefully acknowledge the DFG in the frame of the SPP 1051 'Hochfeld-EPR' for financing the presented project. Furthermore, M. Rohrer and O. Brügmann are thanked for initial contributions in building the 180 GHz EPR spectrometer, as well as B. Kinzer and B. Thiem for technical support with the spectrometer. M. Penning de Vries is acknowledged for support in the high-field lab. Furthermore, we thank Prof. H. R. Kalbitzer's group for providing the Ras proteins as well as Prof. J. Stubbe's group for providing the RNR samples.

## REFERENCES

1. Weber RT, Disselhorst JAJM, Prevo LJ, Schmidt J, Wenckebach WT. *J. Magn. Reson.* 1989; **81**: 129.
2. Bresgunov AY, Dubinskii A, Krimov VN, Petrov YG, Poluektov OG, Lebedev YS. *Appl. Magn. Reson.* 1991; **2**: 715.
3. Prisner TF, Un S, Griffin RG. *Isr. J. Chem.* 1992; **32**: 357.
4. Prisner T, Rohrer M, Moebius K. *Appl. Magn. Reson.* 1994; **7**: 167.
5. Höfer P, Maresch GG, Schmalbein D, Holczer K. *Bruker Rep.* 1996; **142**: 15.
6. Gromov I, Krymov V, Manikandan P, Arieli D, Goldfarb D. *J. Magn. Reson.* 1999; **139**: 8.
7. Pashenko SV, Proskuryakov II, Germano M, van Gorkum HJ, Gast P. *Chem. Phys.* 2003; **294**: 439.
8. Grinberg O, Berliner L. *Very High Frequency ESR/EPR*, vol. 22, Grinberg O, Berliner L (eds). Plenum: New York, 2005.
9. Prisner TF. *Adv. Magn. Opt. Reson.* 1997; **20**: 245.
10. Rohrer M, Brügmann O, Kinzer B, Prisner TF. *Appl. Magn. Reson.* 2001; **21**: 257.
11. Blok H, Disselhorst JAJM, Orlinskii SB, Schmidt J. *J. Magn. Reson.* 2004; **166**: 92.
12. Kutter C, Moll HP, van Toll J, Zuckermann H, Maan JC, Wyder P. *Phys. Rev. Lett.* 1995; **74**(15): 2915.

13. Bennati M, Farrar CT, Bryant JA, Inati SJ, Weis V, Gerfen GJ, Riggs-Gelasco P, Stubbe J, Griffin RG. *J. Magn. Reson.* 1999; **138**: 232.
14. Disselhorst JAJM, van der Meer H, Poluektov OG, Schmidt J. *J. Magn. Reson.* 1995; **116**(A): 183.
15. Goldfarb D, Krymov V. W-Band pulsed ENDOR of transition metal centers in orientationally disordered systems and single crystals. In *Very High Frequency (VHF) ESR/EPR*, Grinberg O, Berliner L (eds). Plenum: New York, 2005.
16. Blok H, Disselhorst JAJM, van der Meer H, Orlinskii SB, Schmidt J. *J. Magn. Reson.* 2005; **173**: 49.
17. Epel B, Manikandan P, Kroneck H, Goldfarb D. *Appl. Magn. Reson.* 2001; **21**: 287.
18. Bennebroek MT, Schmidt J. *J. Magn. Reson.* 1997; **128**: 199.
19. Reed GH, Markham GD. *Biol. Magn. Res.* 1984; **6**: 73.
20. Farrar CT, Hall DA, Gerfen GJ, Inati SJ, Griffin RG. *J. Chem. Phys.* 2001; **114**(11): 4922.
21. Denysenkov V, Prisner TF, Stubbe J, Bennati M. *Appl. Magn. Reson.* in press.
22. Moebitz H, Hertel MM, Bennati M, Boll M. *Biochemistry* submitted.
23. Davies ER. *Phys. Lett.* 1974; **47A**: 1.
24. Grupp A, Mehring M. Pulsed ENDOR Spectroscopy in Solids. In *Modern Pulsed and CW Electron Spin Resonance*, Kevan L, Bowman M (eds). Wiley: New York, 1990; 195.
25. Millhauser GL, Freed JH. *J. Chem. Phys.* 1984; **81**: 37.
26. Wittinghofer A, Waldmann H. *Angew. Chem. Int. Ed.* 2000; **39**: 4192.
27. Spoerner M, Prisner TF, Bennati M, Hertel MM, Weiden N, Schweins T, Kalbitzer HR. *Magn. Reson. Chem.* 2005; **43**(S1): S74–S83.
28. Rohrer M, Prisner T, Brügmann O, Käss H, Spoerner M, Wittinghofer A, Kalbitzer HR. *Biochemistry* 2001; **40**: 1884.
29. Bennati M, Hertel M, Fritscher J, Prisner TF, Weiden N, Dinse KP, Hofweber R, Spoerner M, Horn G, Kalbitzer HR. *Biochemistry* submitted.
30. Morrissey SR, Horton TE, DeRose VJ. *J. Am. Chem. Soc.* 2000; **122**: 3473.
31. Tan X, Bernando M, Thomann H, Scholes CP. *J. Chem. Phys.* 1992; **98**(7): 5147.
32. Carmieli R, Manikandan P, Kalb AJ, Goldfarb D. *J. Am. Chem. Soc.* 2001; **123**: 8378.
33. Milov AD, Ponomarev AB, Tsvetkov YD. *Chem. Phys. Lett.* 1984; **110**: 67.
34. Bennati M, Weber A, Antonic E, Perlstein D, Robblee J, Stubbe J. *J. Am. Chem. Soc.* 2003; **125**: 14 988.
35. Högborn M, Galander M, Andersson M, Kolberg M, Hofbauer W, Lassmann G, Nordlund P, Lendzian F. *PNAS* 2003; **100**: 3209.
36. Hofbauer W, Earle KA, Dunnam CR, Moscicki JK, Freed JH. *Rev. Sci. Instrum.* 2004; **75**(5): 1194.
37. Rohrer M, Plato M, MacMillan F, Grishin Y, Lubitz W, Möbius K. *J. Magn. Reson.* 1995; **116**: 59.